

Scheme 1 Hypotheses for inhibition of [FeFe]-hydrogenases by CH_2O .

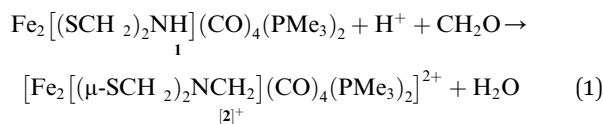
The amine pathways, which involve standard organic reactions, might be relevant to what Bachmeier *et al.* refer to as “matrix” formaldehyde, *i.e.*, unselective binding of formaldehyde in the vicinity of the active site. The Fe-centered reactions are preceded in organometallic chemistry, although not necessarily with iron. Bachmeier *et al.* favor this hypothesis. The third pathway, for which we provide evidence, involves covalent linking the amine and distal iron with a methylene bridge, locking up the $[\text{2Fe}]_{\text{H}}$ active site.

The model complexes used in this paper are $\text{Fe}_2[(\mu\text{-SCH}_2)_2\text{-NH}](\text{CO})_4\text{L}_2$, where $\text{L} = \text{PMe}_3$ and CN^- . These models feature the authentic azadithiolate cofactor bound to a pair of $\text{Fe}(\text{CO})_2\text{L}$ centers. Such complexes are functional models in that they undergo protonation to give hydrides and are redox-active.¹⁷

Results and discussion

$[\text{Fe}_2[(\mu\text{-SCH}_2)_2\text{NCH}_2](\text{CO})_4(\text{PMe}_3)_2]^+$

Solutions of $\text{Fe}_2[(\mu\text{-SCH}_2)_2\text{NH}](\text{CO})_4(\text{PMe}_3)_2$ (**1**) were found to react with a mixture of HBF_4 and paraformaldehyde to give $[\text{Fe}_2[(\mu\text{-SCH}_2)_2\text{NCH}_2](\text{CO})_4(\text{PMe}_3)_2]^+$ (**[2]⁺**). Using stoichiometric amounts of the three reagents, the conversion proceeds rapidly and in good yields at room temperature. These conditions are compatible with those reported for the enzyme. The formula of **[2]⁺** was initially determined by ESI-MS, which showed a strong parent ion (eqn (1)).



In a control experiment, the reaction of the propane-dithiolate $\text{Fe}_2(\mu\text{-S}_2\text{C}_3\text{H}_6)(\text{CO})_4(\text{PMe}_3)_2$ with HBF_4 and paraformaldehyde afforded only the well-known hydride $[\text{HFe}_2(\mu\text{-S}_2\text{C}_3\text{H}_6)(\text{CO})_4(\text{PMe}_3)_2]^+$,¹⁸ the formaldehyde had no effect.

The structure of **[2]⁺** was determined by an X-ray crystallographic study of its $\text{BAR}^{\text{F}}_4^-$ salt ($\text{Ar}^{\text{F}} = \text{C}_6\text{H}_3\text{-3,5-(CF}_3)_2$) (Fig. 2). The two PMe_3 ligands are *trans*-dibasal. Fe1 has an $\text{S}_2(\text{CO})_2(\text{-PMe}_3)(\text{alkyl})$ coordination sphere. The ligand–Fe1–ligand angles are suitable for octahedral coordination, as appropriate for Fe(II). The proximal Fe center Fe2 occupies a $\text{S}_2(\text{CO})_2(\text{PMe}_3)$ coordination sphere. Its coordination number is ambiguous

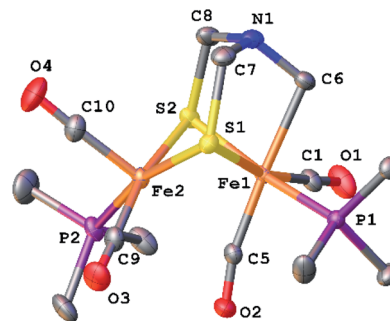


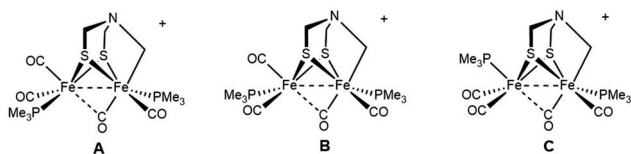
Fig. 2 Structure of $[\text{Fe}_2[(\mu\text{-SCH}_2)_2\text{NCH}_2](\text{CO})_4(\text{PMe}_3)_2]\text{BAR}^{\text{F}}_4^-$ ($[\text{2}]\text{BAR}^{\text{F}}_4^-$) with thermal ellipsoids shown at 50% probability. H atoms and $\text{BAR}^{\text{F}}_4^-$ have been omitted for clarity. Selected distances and angles (Å and °): Fe1–Fe2, 2.5934(3); Fe1–C5, 1.796(2); Fe2–C5, 2.559(2); Fe1–C6, 2.168(2); N1–C6, 1.441(2); N1–C7, 1.431(3); N1–C8, 1.432(2); Fe1–C5–O2, 167.8(2); Fe1–C1–O1, 177.9(2).

because one CO, primarily bound to Fe1, is semi-bridging: Fe1–CO = 1.796(2) and Fe2–CO = 2.559(2) Å. The Fe1–C5–O2 angle for the semi-bridging CO ligand is 167.8(2)°, suggesting that Fe2 is weakly Lewis acidic. Analogous to terminal hydride derivatives of $\text{Fe}_2^{\text{II}}(\mu\text{-SR})_2$ complexes,^{19,20} the ligand *trans* to alkyl is CO. In a related thioaldehyde complexes²¹ $\text{Fe}_2(\mu\text{-SR})(\mu\text{-}\eta^2\text{-SCHR}^{\prime})(\text{diphosphine})(\text{CO})_4$, CO is also *trans* to alkyl.²²

The NMR data for **[2]⁺** are consistent with a stereo-rigid, chiral structure. For example, the ¹³C NMR spectrum shows four CO signals, three signals in the δ 211.45–210.70 region assigned to terminal CO groups, and one signal at δ 201.8 assigned to the semi-bridging CO. These ¹³CO signals are all coupled to ³¹P ($J_{\text{PC}} = 19.7$ Hz), characteristic of CO *cis* to PMe_3 .²³ The ¹³C NMR signal for the formaldehyde-derived methylene appears at δ 75.77. Its ¹H NMR spectrum shows multiplets at δ 5.52 and 4.79, assigned to the diastereotopic CH_2 protons. The four SCH_2N protons are nonequivalent, also consistent with the low symmetry of the complex. Spin-saturation transfer experiments, which probes the exchange of signals at rates faster than $1/T_1$, were conducted on **[2]⁺**. Saturation of one of the SCH_2 signals centered at δ 3.84 ($T_1 = 1.17$ s for SCH_2) or one of the NCH_2Fe signals at δ 4.79 ($T_1 = 1.31$ s for NCH_2Fe) revealed that these sites do not exchange on the seconds time scale (Fig. S14 and S15[†]). As discussed below, ¹³C-labeling reveals that all three methylene groups do in fact exchange over the course of several minutes.

The ³¹P NMR data for **[2]⁺** reveal the presence of a mixture of three (chiral) diastereoisomers in a 5 : 1 : 1 ratio. The minor diastereoisomers are not evident in the above-discussed ¹³C NMR data. If we assume that Fe1 center has CO *trans* to the alkyl ligand, as mentioned above, the three isomers result from the three diastereomeric sites on Fe2:

We assume that the main isomer (A) has *trans*-dibasal phosphine ligands as established by X-ray crystallography. This dominant and one minor isomer (B) both show ³¹P–³¹P coupling (respectively, $J = 7.4, 7.6$ Hz). The two ³¹P NMR signals for the third isomer (minor, C) show no ³¹P, ³¹P coupling. Its unique (non)coupling is consistent with a unique structure, *i.e.*, apical–basal disposition of the PMe_3 ligands.

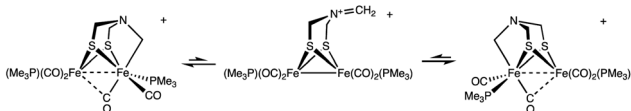


The entirety of the NMR data is accommodated by an exchange process involving reversible scission of the Fe–C bond, concomitant with regeneration of an Fe(I)Fe(I) species. Scission of the CH₂–Fe bond introduces an effective plane of symmetry such that the two Fe(I) centers become equivalent (Scheme 2). Further relevant to stereodynamics, the exchange for the FeL₃ sites is rapid in Fe(I)Fe(I) complexes, whereas biotetrahedral Fe(II)Fe(II) complexes are more rigid.²⁴

Evidence of the process shown in Scheme 2 is provided by ³¹P NMR spin saturation experiments. The *T*₁ of the signal at δ 9.45 was determined to be 8.2 s, and the exchange rate was *k* = 0.85 s⁻¹. Saturation of either of the signals at δ 22.45 or 9.45 resulted in collapse of the other five ³¹P NMR signals (Fig. 3).

Mechanistic studies

Since Brønsted acids are required for the conversion of **1** to [2]⁺, we examined the ammonium complex [Fe₂[(μ -SCH₂)₂-NH₂](CO)₄(PMe₃)₂]⁺ ([1H]⁺). These results, which overlap with those reported earlier by Pickett,²⁵ are rather fundamental and merit thorough analysis. ¹H and ³¹P NMR spectra confirm that [1H]⁺ is stable in solution for days. Treating a CH₂Cl₂ solution of [1H]BF₄ with NaBAR₄^F induced tautomerization to the hydride [HFe₂[(μ -SCH₂)₂NH](CO)₄(PMe₃)₂]⁺ ([H1]⁺). According to IR measurements, the tautomerization is complete after 3 h at room temperature (eqn (2)).



Scheme 2 Proposed stereodynamics for [2]⁺. The process would proceed with racemization.

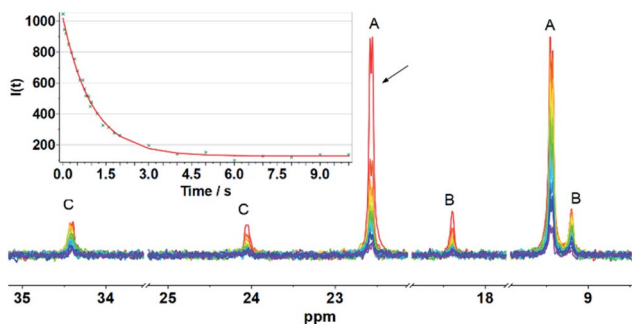
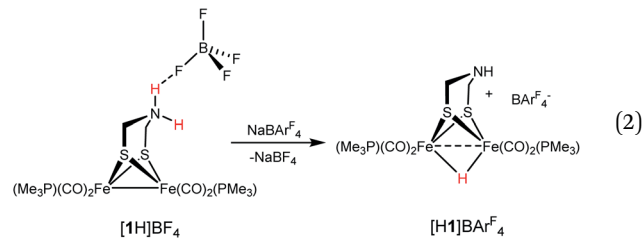


Fig. 3 ³¹P NMR spin saturation transfer spectra of [2]BAR₄^F at 298 K in CD₂Cl₂. Irradiation of the signal at δ 22.59. *T*₁ = 8.2 s for the resonance at δ 9.45. Inset: graph of intensity (*I*) of the δ 9.45 peak vs. irradiation time at δ 22.59. Fitting: $I_t = I_0 \times \{1/(1 + \tau/8.2)\} \times \exp[-t \times (1/8.2 + 1/\tau)] + 1/(1 + 8.2/\tau)$, where $\tau = 1.17$ s, *k* = 1/ τ = 0.85 s⁻¹.



The ¹H NMR spectrum for [H1]⁺ matches published data for related salts.¹⁸ The anion-dependent tautomerization reflects the stabilization of ammonium centers by hydrogen-bonding to BF₄⁻, which persists in solution.²⁶ One consequence of the ion-pairing (or its absence in the case of BAR₄^{F-}) is that the proton-induced reaction of **1** with CH₂O is sensitive to the identity of the acid: H(OEt₂)BF₄ cleanly gives [2]⁺ but H(OEt₂)₂BAR₄^F, depending on the specific conditions, can afford significant quantities of the hydride [H1]⁺.

X-ray crystallography verified the extensive hydrogen-bonding in solid [H1]⁺ (Fig. 4). The asymmetric unit consists of three ion pairs; two cations have *trans*-dibasal phosphine ligands, one is apical-basal. All NH centers are hydrogen bonded to BF₄⁻. The F⋯N distances range from 1.97–2.54 Å with the average distance of 2.22 Å.²⁷

The hydroxymethylation of secondary amines by formaldehyde is well studied.²⁸ When a solution of **1** was treated with CH₂O in the absence of acid, only subtle shifts (<5 cm⁻¹) were observed in the IR spectrum in the ν_{CO} region. It is known, however, that ν_{CO} is relatively insensitive to substituents on nitrogen of the amine. For example, in this work we found that the ν_{CO} bands for Fe₂[(μ -SCH₂)₂NR](CO)₄(PMe₃)₂ are almost identical for R = H (1983, 1943, 1899 cm⁻¹) and R = Me (1983, 1945, 1909, 1894 cm⁻¹). ¹H NMR spectroscopy proved to be a more sensitive indicator of the interaction of **1** and CH₂O. A 1 : 0.25 mixture of these reactants generates ~25% of a new species that we assign to the hydroxymethyl derivative Fe₂[(μ -

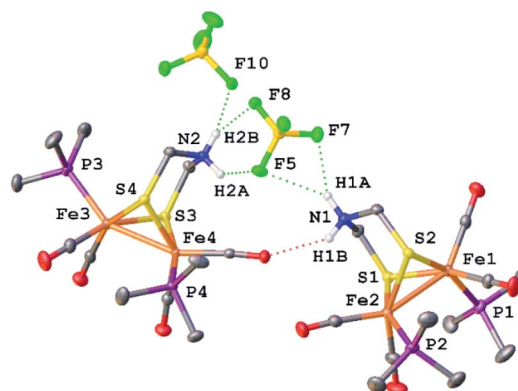


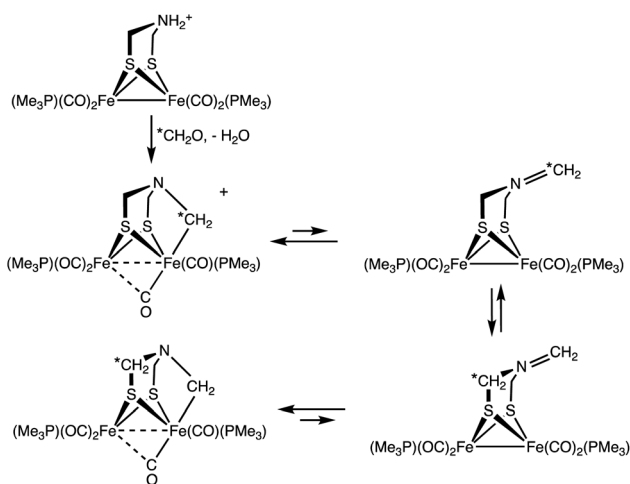
Fig. 4 Structure of [Fe₂[(μ -SCH₂)₂NH₂](CO)₄(PMe₃)₂]BF₄ with thermal ellipsoids shown at 50% probability. H atoms except for the NH₂ centres have been omitted for clarity. Two of the three ion pairs in the asymmetric unit are shown. Notice the presence of stereoisomers of [H1]⁺. Selected distances (Å): Fe1–Fe2, 2.5689(3); Fe3–Fe4, 2.5444(3); H1A–F5, 2.54(2); H1A–F7, 2.10(2); H2A–F5, 2.30(2); H2B–F8, 2.41(2); H2B–F10, 2.00(2).

SCH₂)₂NCH₂OH](CO)₄(PMe₃)₂. The same species is observed with ¹³CH₂O under otherwise identical conditions. In that experiment, the SCH₂N groups did not show any enrichment. When **1** and CH₂O were mixed in a 1 : 1 ratio, several species are observed, Fe₂[(μ-SCH₂)₂NCH₂OH](CO)₄(PMe₃)₂, some unreacted **1**, and what appears to be Fe₂[(μ-SCH₂)₂-N(CH₂O)_{*n*}CH₂OH](CO)₄(PMe₃)₂. Equilibration of these species is rapid, since the mixture reacts with 1 equiv. of HBF₄ to cleanly give [2]⁺. No reaction was evident when **1** was treated with PhCHO, in the presence or absence of HBF₄.

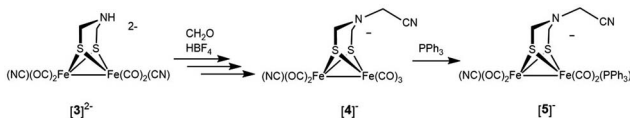
Treatment of a solution of ¹³CH₂O and **1** with H(Et₂O)₂BAR^F₄ gave [¹³2]⁺ with selective formation of the Fe-¹³CH₂ isotopomer. Interestingly, this label exchanges with the other methylene groups in the complex over the course of hours (Scheme 3). The kinetics of exchange are first order in [2]⁺ up to about 90% conversion, which points to an intramolecular process. The NMR data show that this ¹³CH₂/¹²CH₂ exchange affects the diastereotopic SCH₂ groups equally. We suggest that exchange occurs for the Fe(I)Fe(I) species where the diastereomerization is rapid. The ESI-MS of the product of the labelling shows only singly labelled [2]⁺. Intermolecular processes would be expected to yield detectable levels of doubly labeled product.

Reaction of [Fe₂[(μ-SCH₂)₂NH](CN)₂(CO)₄]²⁻ with CH₂O/HBF₄

The reaction of paraformaldehyde with [Fe₂[(μ-SCH₂)₂-NH](CN)₂(CO)₄]²⁻ ([3]²⁻) was investigated because this complex resembles the [2Fe]_H active site, which is also a dicyanide. In the presence of one equiv. of HBF₄, [3]²⁻ converts to the ammonium derivative, which is stable in MeCN solution for several minutes



Scheme 3 Synthesis of [2]⁺ using ¹³CH₂O, showing site exchange.



Scheme 4 Pathway for formation of [Fe₂[(μ-SCH₂)₂-NCH₂CN](CN)(CO)₄(PPh₃)]⁻ ([5]⁻).

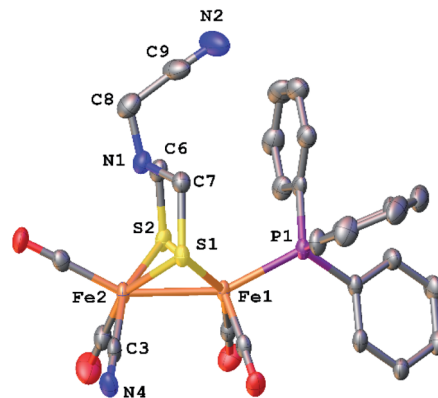


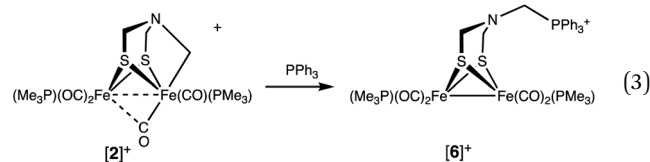
Fig. 5 Structure of Et₄N[Fe₂[(μ-SCH₂)₂NCH₂CN](CN)(CO)₄(PPh₃)] (Et₄N[5]) with thermal ellipsoids shown at 50% probability. H atoms and the Et₄N⁺ cation have been omitted for clarity. Selected distances (Å): Fe1–Fe2, 2.5263(8); Fe2–C3, 1.928(5); C3–N4, 1.148(6); C9–N2, 1.144(8).

prior to irreversible tautomerization to the hydride (Fig. S39[†]). Addition of paraformaldehyde to [3H]⁻ gives one main product, which we assign as the pentacarbonyl [Fe₂[(μ-SCH₂)₂-NCH₂CN](CN)(CO)₅]⁻ ([4]⁻). This formula is supported by ESI-MS analysis. Attempted purification of [4]⁻ was unsuccessful, however its FT-IR spectrum is very similar to that for [Fe₂[(μ-S₂-C₃H₆)](CN)(CO)₅]⁻. When ¹³CH₂O was used, the singly labeled product was generated according to ESI-MS. We propose that [4]⁻ arises by reductive elimination of the nitrile from [Fe₂[(μ-SCH₂)₂NCH₂](CN)₂(CO)₄]⁻ followed by CO-scavenging (Scheme 4).

The phosphine derivative of [4]⁻ was obtained when the reaction of [3]²⁻ with CH₂O was conducted in the presence of PPh₃ (Scheme 4). The ³¹P NMR signal of this product at δ 60.1 indicates coordination of PPh₃, leading to the formula [Fe₂[(μ-SCH₂)₂-NCH₂CN](CN)(CO)₄(PPh₃)]⁻ ([5]⁻). In the FT-IR spectrum of [5]⁻, the ν_{CO} bands are shifted by 21 cm⁻¹ toward high energy compared to dicyanide complex [3]²⁻. The structure of [5]⁻ was verified by X-ray crystallography (Fig. 5), which confirms the presence of a conventional [Fe₂(μ-SR)₂(CN)(CO)₄(PPh₃)]⁻ complex,²⁹ and, most importantly, the presence of the cyanomethyl substituent.

Reactions of methylenated FeFe complex with nucleophiles

The Fe–CH₂N bond in [2]⁺ is electrophilic. For example, treating [2]⁺ with PPh₃ cleanly gave [Fe₂[(μ-SCH₂)₂-NCH₂PPh₃](CO)₄(PMe₃)₂]⁺BF₄⁻ ([6]⁺), the result of C–P bond formation. Dealkylation of Fe involves reduction to an [Fe(I)]₂ complex (eqn (3)).



The PMe₃ ligands in [6]⁺ appear equivalent, as is typical for related [Fe(I)]₂ complexes. The presence of a phosphonium

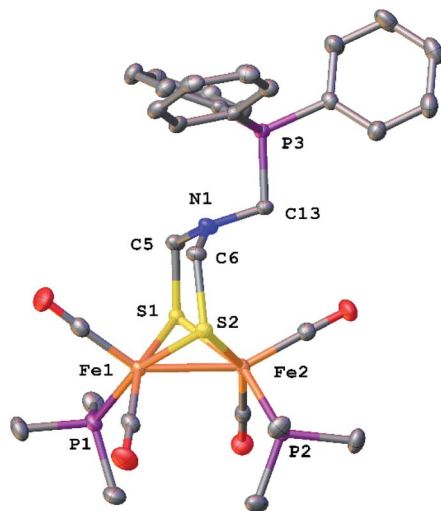
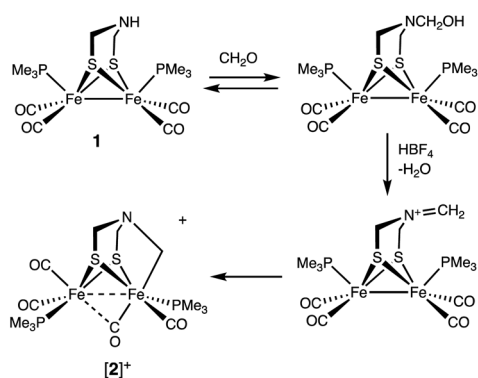
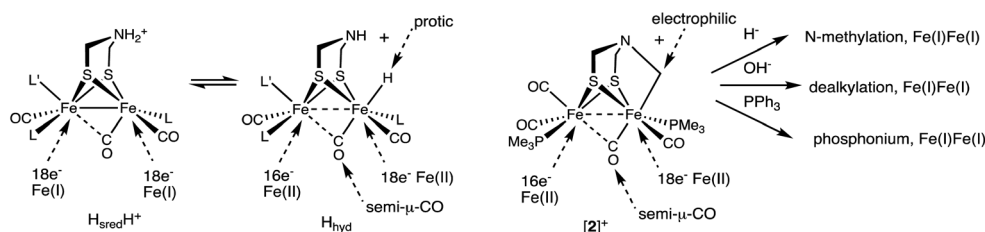


Fig. 6 Structure of $[\text{Fe}_2(\mu\text{-SCH}_2)_2\text{NCH}_2\text{PPh}_3](\text{CO})_4(\text{PMe}_3)_2\text{BF}_4$ (**6**) with thermal ellipsoids shown at 50% probability. H atoms and BF_4^- anion have been omitted for clarity. Selected distances (Å): Fe1–Fe2, 2.5706(4); N1–C5, 1.436(3); N1–C6, 1.445(3); N1–C13, 1.449(3).



Scheme 5 Proposed pathway for the methylenation of **1**.

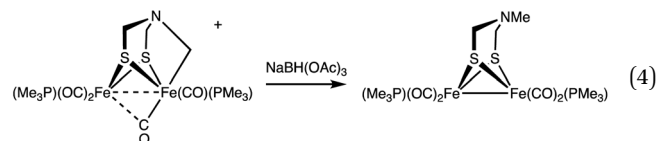
center is indicated by the ^{31}P NMR singlet at δ 9.17, much higher field than δ 65.7 for $\text{Fe}_2(\mu\text{-S}_2\text{C}_3\text{H}_6)(\text{CO})_5(\text{PPh}_3)$.³⁰ In the region assigned to NCH_2P , the ^1H NMR spectrum features a broad signal at δ 4.90. The broadness is associated with the nonequivalent protons, each of which is coupled to ^{31}P . The IR spectrum of **6** also agrees with reduction of Fe(II)Fe(II) to Fe(I)Fe(I) : ν_{CO} shifts to lower frequency by 55 cm^{-1} (1978, 1948, 1903 cm^{-1}). These frequencies are comparable to those in **1**.



Scheme 6 Comparison of the $[\text{2Fe}]_{\text{H}}$ centers in the $\text{H}_{\text{sred}}\text{H}^+$ and H_{hyd} states ($\text{L} = \text{CN}^-$) and $[\text{2}]^+$, including its reactions.

The structure of **6** was verified by X-ray crystallography (Fig. 6). The complex is a conventional $\text{Fe}_2(\mu\text{-SR})_2(\text{CO})_{6-x}\text{L}_x$ butterfly. The bulky phosphonium substituent is distant from the Fe_2 core.

Conversion of $[\text{2}]^+$ back to **1** was induced upon treatment with Et_4NOH . From this reaction, **1** was recovered in 40% yield after purification by column chromatography. The electrophilic nature of the $\text{Fe}-\text{CH}_2$ bond is also supported by the reaction of $[\text{2}]^+$ with $\text{BH}(\text{OAc})_3^-$, a mild hydride donor. In this case, $\text{Fe}_2[(\mu\text{-SCH}_2)_2\text{NMe}](\text{CO})_4(\text{PMe}_3)_2$ was obtained in good yield (eqn (4)).



Conclusions

As a specific conclusion, this work provides a plausible model for the inhibition of $[\text{FeFe}]$ -hydrogenases by formaldehyde. The methylene group donated by formaldehyde occupies both substrate binding sites, amine and the distal Fe. The methylation proceeds by addition of the aldehyde to the secondary amine followed by generation of the iminium cation, which oxidatively adds to one of the Fe(I) centers, oxidizing the diiron site by $2e^-$ (Scheme 5). Many examples exist for the addition of iminium cations to low-valent metals.³¹ The methylation reaction does not proceed from the diiron μ -hydride. In accord with the results of Bachmeier *et al.*,¹³ the methylation is selective for reduced state(s) of the diiron center, as required for oxidative addition.

Complex $[\text{2}]^+$ represents a rare mimic of a terminal hydride for the $[\text{FeFe}]$ -hydrogenases. Normally terminal hydrides of synthetic diiron dithiolates rapidly isomerize,²⁰ which precludes extensive characterization of this key intermediate.³² In the Mulheim mechanism, the diferrous terminal hydride corresponds to H_{hyd} state, defined as $[\text{4Fe}-4\text{S}]^+-\text{Fe}_p(\text{II})\text{-amine-Fe}_d(\text{II})\text{H}$. In this state, the hydride is protic, being reversibly deprotonated by the amine cofactor. Consistent with this model, the alkyl ligand in $[\text{2}]^+$ is electrophilic. Furthermore, analogous to the reversible deprotonation of H_{hyd} , $[\text{2}]^+$ reversibly dealkylates (see Scheme 2) to give a Fe(I)Fe(I) species as proposed for the $\text{H}_{\text{sred}}\text{H}^+$ state. Complex $[\text{2}]^+$ exists as an equilibrium mixture of three isomers. The finding that these isomers are separated by

less than ~ 1 kcal mol⁻¹, shows that stereochemistry of the other ligands on the diiron dithiolate has little influence on the Fe-alkyl bond (and by inference Fe-hydride bond). Also like H_{hyd} state, [2]⁺ has a highly unsymmetrical semi-bridging CO *trans* to R (= alkyl, hydride) on the distal Fe is persistent. In a future paper we plan to describe the redox chemistry of this electrophilic Fe(II)Fe(II) in our quest to further probe analogues of the elusive H_{hyd}H⁺ state.

As established by its reactions with a range of nucleophiles (Scheme 6), [2]⁺ presents opportunities for appending the Fe₂(μ-SR)₂ center to other scaffolds.

The susceptibility of [2]⁺ to nucleophilic attack is reminiscent of Co(III)-alkyls as represented by vitamin B₁₂ and its derivatives and models.^{33,34} Given the vast chemistry of B₁₂ mimics, it is possible that a wide range of diiron alkyl chemistry awaits discovery and development.

Experimental

Materials and methods

Reactions were conducted in stirred solutions or slurries under nitrogen at room temperature unless otherwise indicated. Sample work-up routinely included rinsing solids with Et₂O or pentane and storage under vacuum to remove traces of solvent. All reactions and purifications were conducted using standard Schlenk techniques or in an MBraun glovebox under N₂. Solvents were purified using solvent purification system equipped with alumina filtration column. CD₂Cl₂ was degassed by freeze-pump-thaw cycles and dried using 4 Å molecular sieves. ¹H, ³¹P{¹H}, and ¹³C NMR spectra were recorded on Varian 500, Varian 600, Bruker 500, or Bruker Ascend 600 MHz spectrometers. Chemical shifts (δ/ppm) are referenced to residual solvent peak (5.32 ppm for ¹H and 53.84 ppm for ¹³C in CD₂Cl₂). Chemical shifts (δ/ppm) for ³¹P{¹H} NMR were calibrated using 85% H₃PO₄ as an external reference (0 ppm). Solution IR spectra were recorded on a PerkinElmer Spectrum 100 FTIR spectrometer. Elemental analysis was performed utilizing an Exeter CE-440 elemental Analyzer. A Waters Micromass Quattro II spectrometer was used to acquire ESI-MS data. Crystallographic data were collected on a Bruker D8 Venture kappa diffractometer equipped with a Photon II CPAD detector. An Iμs Microfocus Mo source (λ = 0.71073 Å) coupled with a multi-layer mirror monochromator provided the incident beam. Literature procedures were followed for the synthesis of (Et₄N)₂[Fe₂(μ-SCH₂)₂NH](CN)₂(CO)₄,³⁵ Fe₂[(μ-SCH₂)₂-NH](CO)₄(PMe₃)₂,²⁵ and Fe₂[(μ-SCH₂)₂NMe](CO)₄(PMe₃)₂.^{23,25} Other chemicals were purchased from commercial sources and used without further purification.

[Fe₂[(μ-SCH₂)₂NH₂](CO)₄(PMe₃)₂]BF₄ ([1H]BF₄). To a solution of Fe₂[(μ-SCH₂)₂NH](CO)₄(PMe₃)₂ (**1**) (100 mg, 0.21 mmol) in 10 mL of CH₂Cl₂ was added HBF₄·Et₂O (34 mg, 0.21 mmol). After 10 min, the solution was concentrated to ~ 1 mL, and a red solid was precipitated upon addition of 10 mL of Et₂O. Yield: 95 mg (81%). ¹H NMR (500 MHz, CD₂Cl₂): δ 6.36 (s, 2H, NH₂), 3.49 (s, 4H, (SCH₂)₂N), 1.57 (d, 18H, P(CH₃)₃). ³¹P{¹H} NMR (202 MHz, CD₂Cl₂): δ 26.24. IR (CH₂Cl₂): ν_{CO} = 2000, 1963,

1923 cm⁻¹. Anal. calcd for C₁₂H₂₅BF₄Fe₂NO₄P₂S₂: C, 25.2; H, 4.41; N, 2.45. Found, C, 25.06; H, 4.05; N, 2.32.

[HFe₂[(μ-SCH₂)₂NH](CO)₄(PMe₃)₂]BAR^F₄ ([1H]BAR^F₄). To a solution of [1H]BF₄ (40 mg, 0.070 mmol) in 4 mL of CH₂Cl₂ was added solid NaBAR^F₄ (73 mg, 0.070 mmol). IR spectra showed full conversion to [1H]BAR^F₄ after 3 h. The reaction mixture was filtered through Celite and evaporated. The residue was recrystallized using CH₂Cl₂/pentane at -30 °C to give a red crystalline solid. Yield: 85% (79.9 mg). ¹H NMR (500 MHz, CD₂Cl₂): δ 7.72 (s, 8H, ArH), 7.57 (s, 4H, ArH), 4.13 (s, 4H, SCH₂), 2.32 (p, *J* = 8.8 Hz, 1H, NH), 1.55 (d, *J*_{PH} = 10.2 Hz, 18H, P(CH₃)₃), -14.52 (t, *J*_{PH} = 21.5 Hz, 1H). ³¹P{¹H} NMR (202 MHz, CD₂Cl₂): δ 21.81. IR (CH₂Cl₂): ν_{CO} = 2033, 1992 cm⁻¹. ESI-MS *m/z* calcd for [M⁺], 483.9. Found, 484.0. Anal. calcd for C₄₄H₃₅-BF₂₄Fe₂NO₄P₂S₂: C, 39.25; H, 2.62; N, 1.04. Found, 39.23; H, 2.57; N, 1.27.

[Fe₂[(μ-SCH₂)₂NCH₂](CO)₄(PMe₃)₂]BF₄ ([2]BF₄). A solution of Fe₂[(μ-SCH₂)₂NH](CO)₄(PMe₃)₂ (**1**) (200 mg, 0.41 mmol) in 20 mL of CH₂Cl₂ was treated with CH₂O (25 mg, 0.83 mmol). After stirring this mixture for 1 h, HBF₄·Et₂O (67 mg, 0.41 mmol) was added by syringe. The color of the reaction mixture immediately changed from red to dark brown. After a further 30 min, the mixture was analyzed by IR spectroscopy, which showed that the bands for **1** were replaced by new bands at higher energy. The solution was concentrated to 5 mL under vacuum. Addition of 40 mL of Et₂O precipitated the black solid. Yield: 207 mg (86%). ¹H NMR (500 MHz, CD₂Cl₂): δ 5.51 (br, 1H, NCH₂Fe), 5.14 (br, 1H, NCH₂Fe), 3.95 (br, 2H, SCH₂), 3.31 (br, 2H, SCH₂), 1.69 (br, 18H, P(CH₃)₃). ³¹P{¹H} NMR (203 MHz, CD₂Cl₂): δ 35.00 (br), 24.67, 24.28, 22.70 (br), 8.94 (br). IR (CH₂Cl₂): ν_{CO} = 2044, 2017, 1990, 1942 cm⁻¹. HR-MS (ESI) *m/z* calcd for [M⁺], 495.9321. Found, 495.9312. Elemental analysis was obtained on the BAR^F₄⁻ salt (see next procedure).

[Fe₂[(μ-SCH₂)₂NCH₂](CO)₄(PMe₃)₂]BAR^F₄ ([2]BAR^F₄). A 20 mL vial was loaded with [2]BF₄ (50 mg, 0.086 mmol), 1.0 equiv. of NaBAR^F₄ (88 mg, 0.086 mmol), followed by 5 mL of CH₂Cl₂. After stirring the mixture for 1 h, solvent was removed *in vacuo*. The residue was extracted into 2 mL of CH₂Cl₂. This extract was filtered through Celite and layered with hexane. Dark-brown microcrystals were obtained after 2 days. Yield: 110 mg (95%). ¹H NMR (500 MHz, CD₂Cl₂): δ 7.73 (m, 8H, ArH), 7.57 (s, 4H, ArH), 5.52 (m, 1H, NCH₂Fe), 4.79 (m, 1H, NCH₂Fe), 4.17 (dd, *J* = 11.5, 3.8 Hz, 1H, SCH₂), 3.84 (dd, *J* = 11.8, 8.7 Hz, 1H, SCH₂), 3.25 (dd, *J* = 11.8, 3.4 Hz, 2H, SCH₂), 1.66 (d, *J*_{PH} = 10.3 Hz, 9H, P(CH₃)₃), 1.53 (d, *J*_{PH} = 10.4 Hz, 9H, P(CH₃)₃). ³¹P{¹H} NMR (243 MHz, CD₂Cl₂), three isomers were detected: δ 22.59 (d, *J*_{PP} = 7.3 Hz), 9.45 (d, *J*_{PP} = 7.4 Hz), *trans*-dibasal; 34.46 (d, *J*_{PP} = 7.7 Hz), 24.10 (d, *J*_{PP} = 7.6 Hz), *cis*-dibasal; 18.41 (s), 9.21 (s), apical-basal. ¹³C NMR (126 MHz, CD₂Cl₂): δ 212.37–210.12 (m, *t*-CO), 201.90 (d, *J*_{PC} = 19.7 Hz, μ-CO), 162.18 (q, ¹*J*_{BC} = 49.8 Hz), 135.22, 131.08–128.70 (qq, ²*J*_{CF} = 31.4 Hz, ⁴*J*_{CF} = 2.9 Hz), 125.03 (q, ¹*J*_{CF} = 272.4 Hz), 118.55–116.81 (m), 75.77 (d, ²*J*_{PC} = 12.0 Hz, NCH₂Fe), 58.45 (s, SCH₂), 58.15 (d, ³*J*_{PC} = 5.5 Hz, SCH₂), 18.74 (d, ¹*J*_{PC} = 33.4 Hz, P(CH₃)₃), 16.69 (d, ¹*J*_{PC} = 32.0 Hz, P(CH₃)₃). IR (CH₂Cl₂): ν_{CO} = 2046, 2020, 1992, 1942 (μ-CO). Anal. calcd for C₄₅H₃₆BF₂₄Fe₂NO₄P₂S₂: C, 39.76; H, 2.67; N, 1.03. Found, C,

39.33; H, 2.59; N, 1.09. Single crystals were grown by diffusion of hexane into a CH₂Cl₂ solution.

Reaction of [2]BF₄ with NaBH(OAc)₃. To a solution of [2]BF₄ (15 mg, 0.026 mmol) in 2 mL of MeCN was added NaBH(OAc)₃ (5.5 mg, 0.026 mmol, 1 equiv.). The reaction solution changed from dark brown to red immediately. After a further 10 min, solvent was removed, and the residue was extracted into pentane. Removing the solvent under vacuum gave Fe₂[(μ-SCH₂)₂NMe](CO)₄(PMe₃)₂ as a red solid. Yield: 86% (11 mg). The NMR spectrum of this product matches that of authentic Fe₂[(μ-SCH₂)₂NMe](CO)₄(PMe₃)₂.²⁵ ¹H NMR (500 MHz, CD₂Cl₂): δ 2.91 (s, 4H, SCH₂), 2.10 (s, 3H, NCH₃), 1.49 (d, *J*_{PH} = 9.1 Hz, 18H, P(CH₃)₃). ³¹P{¹H} NMR (202 MHz, CD₂Cl₂): δ 22.81. ESI-MS *m/z* calcd for [M + H]⁺, 497.9. Found, 498.2. IR (CH₂Cl₂): ν_{CO} = 1983, 1945, 1909, 1894 sh cm⁻¹.

[Fe₂[(μ-SCH₂)₂NCH₂PPh₃](CO)₄(PMe₃)₂]BF₄ ([6]BF₄). A solution of PPh₃ (23 mg, 0.086 mmol) in 2 mL of CH₂Cl₂ was added dropwise to a solution of [2]BF₄ (50 mg, 0.086 mmol) in 2 mL of CH₂Cl₂. The color changed from purple to red immediately. After stirring for 10 min, the solution was concentrated to 1 mL. The concentrate was layered with 10 mL of Et₂O, and this biphasic mixture was stored at -30 °C. Red crystals appeared after 24 h. Yield: 66 mg (91%). ¹H NMR (500 MHz, CD₂Cl₂): δ 8.49–7.29 (m, 5H, ArH), 4.90 (s, 2H, NCH₂P), 3.45 (s, 4H, SCH₂), 1.50 (d, *J*_{PH} = 9.2 Hz, 18H, P(CH₃)₃). ³¹P{¹H} NMR (203 MHz, CD₂Cl₂): δ 24.15, 9.18. IR (CH₂Cl₂): ν_{CO} = 1978, 1948, 1903. ESI-MS: *m/z* calcd for [M⁺ - CO], 730.4. Found, 730.0. Anal. calcd for C₃₁H₃₉BF₄Fe₂NO₄P₃S₂: C, 44.05; H, 4.65; N, 1.66. Found, C, 43.63; H, 4.96; N, 1.80. Single crystals were grown by diffusion of Et₂O into a CH₂Cl₂ solution at -30 °C.

Reaction of [Fe₂[(μ-SCH₂)₂NCH₂](CO)₄(PMe₃)₂]BF₄ ([2]BF₄) with Et₄NOH. To a solution of [2]BF₄ (40 mg, 0.069 mmol) in 2 mL of THF was added Et₄NOH (10.1 mg, 0.069 mmol, 1.0 equiv., 20% wt aqueous solution). After 2 h, the reaction mixture was evaporated to dryness. The residue was extracted into 1 mL of CH₂Cl₂. This extract was filtered through Celite to remove Et₄NBF₄. A concentrate of this filtrate was purified by column chromatography on silica gel eluting with Et₂O/pentane. Yield of **1**: 13 mg (40%). Product as **1** was identified by FT-IR and ¹H NMR spectroscopy, as well as TLC.

Et₄N[Fe₂[(μ-SCH₂)₂NCH₂CN](CN)(CO)₄(L)] ((Et₄N[4] (L = CO) and Et₄N[5] (L = PPh₃))

Et₄N[4]. A solution of (Et₄N)₂[Fe₂[(μ-SCH₂)₂NH](CN)₂(CO)₄] (50 mg, 0.078 mmol) in MeCN was treated with paraformaldehyde (4.7 mg, 0.016 mmol). After stirring this mixture for 2 h, a solution of H(OEt₂)BF₄ (13 mg, 0.078 mmol) in 2 mL of MeCN was added dropwise. The color of the reaction mixture changed from deep red to dark brown immediately. FT-IR: ν_{CO} = 2038, 2000, 1980, 1945, 1935 (sh), 1912 cm⁻¹; ν_{CN} = 2108 cm⁻¹. ESI-MS: *m/z* calcd for [M⁻], 423.8. Found, 423.8. When the experiment was conducted in the presence of ¹³CH₂O, the FT-IR spectrum was the same. ESI-MS: *m/z* calcd for [M⁻], 424.8. Found, 424.8.

Et₄N[5]. The experiment above was repeated using [HPPPh₃]BF₄ (27 mg, 0.078 mmol) in place of H(OEt₂)BF₄. A solution of (Et₄N)₂[Fe₂[(μ-SCH₂)₂NH](CN)₂(CO)₄] (50 mg, 0.078 mmol) in MeCN was treated with paraformaldehyde (4.7 mg, 0.016

mmol). After 2 h, the IR spectrum showed no change in the CO region. A solution of [HPPPh₃]BF₄ (27 mg, 0.078 mmol) in 2 mL of MeCN was then added dropwise. The color of the reaction mixture changed from red to dark brown immediately. After 12 h, the color turned to red again. The mixture was then concentrated to 2 mL, and the concentrate was filtered through Celite and layered with 20 mL of Et₂O. After 2 days at -30 °C, the layered solution yielded a red solid. Yield: 75% (45 mg). ¹H NMR (600 MHz, CD₂Cl₂): δ 7.68–7.66 (m, 6H, ArH) 7.40–7.39 (m, 9H, ArH), 3.17–3.15 (q, 8H, ¹N(CH₂CH₃)₄), 2.57–2.52 (br, 4H, SCH₂), 2.43 (s, 2H, NCH₂CN), 1.25 (t, 12H, ¹N(CH₂CH₃)₄). ³¹P{¹H} NMR (203 MHz, CD₂Cl₂): δ 60.06. ¹³C NMR (151 MHz, CD₂Cl₂): δ 218.28 (CO), 138.69 (d, CN), 133.71 (d, *J*_{PC} = 11.5 Hz, P(C₆H₅)₃), 129.67 (d, *J*_{PC} = 2 Hz, P(C₆H₅)₃), 128.44 (d, *J*_{PC} = 9.0 Hz, P(C₆H₅)₃), 114.82 (NCH₂CN), 53.23 (¹N(CH₂CH₃)₄), 50.64 (SCH₂), 46.77 (NCH₂CN), 8.00 (¹N(CH₂CH₃)₄). IR (CH₂Cl₂): ν_{CO} = 1988, 1950, 1916 cm⁻¹, ν_{CN} = 2081 cm⁻¹. Anal. calcd for C₃₅H₄₁Fe₂N₄O₄PS₂·0.2CH₂Cl₂: C, 52.49; H, 5.18; N, 6.96. Found, C, 52.48; H, 5.42; N, 7.15. ESI-MS: *m/z* calcd for [M⁻], 657.9. Found, 657.9. Single crystals were grown by diffusion of Et₂O into a CH₂Cl₂ solution at room temperature.

Data availability

All experimental and crystallographic data are available in the ESI.†

Author contributions

Methodology, investigation, writing: F. Z.; conceptualisation and writing: T. B. R. Investigation: L. Z. and T. J. W. All authors have given approval to the final version of the manuscript.

Conflicts of interest

There are no conflicts to declare.

Acknowledgements

This work was supported by GM-61153 from the National Institutes of Health.

Notes and references

- H. Land, M. Senger, G. Berggren and S. T. Stripp, Current State of [FeFe]-Hydrogenase Research: Biodiversity and Spectroscopic Investigations, *ACS Catal.*, 2020, **10**, 7069–7086.
- J. T. Kleinhaus, F. Wittkamp, S. Yadav, D. Siegmund and U.-P. Apfel, [FeFe]-Hydrogenases: Maturation and Reactivity of Enzymatic Systems and Overview of Biomimetic Models, *Chem. Soc. Rev.*, 2021, **50**, 1668–1784.
- A. Dutta, A. M. Appel and W. J. Shaw, Designing Electrochemically Reversible H₂ Oxidation and Production Catalysts, *Nat. Rev. Chem.*, 2018, **2**, 244–252.
- Bioinspired Catalysis*, ed. Schollhammer, P. and Weigand, W., Wiley-VCH, Weinheim, 2015.

- 5 R. M. Bullock, J. G. Chen, L. Gagliardi, P. J. Chirik, O. K. Farha, C. H. Hendon, C. W. Jones, J. A. Keith, J. Klosin, S. D. Minter, R. H. Morris, A. T. Radosevich, T. B. Rauchfuss, N. A. Strotman, A. Vojvodic, T. R. Ward, J. Y. Yang and Y. Surendranath, Using Nature's Blueprint to Expand Catalysis with Earth-Abundant Metals, *Science*, 2020, **369**, eabc3183.
- 6 E. J. Reijerse, C. C. Pham, V. Pelmenschikov, R. Gilbert-Wilson, A. Adamska-Venkatesh, J. F. Siebel, L. B. Gee, Y. Yoda, K. Tamasaku, W. Lubitz, T. B. Rauchfuss and S. P. Cramer, Direct Observation of an Iron-Bound Terminal Hydride in [FeFe]-Hydrogenase by Nuclear Resonance Vibrational Spectroscopy, *J. Am. Chem. Soc.*, 2017, **139**, 4306–4309.
- 7 V. Pelmenschikov, J. A. Birrell, C. C. Pham, N. Mishra, H. Wang, C. Sommer, E. Reijerse, C. P. Richers, K. Tamasaku, Y. Yoda, T. B. Rauchfuss, W. Lubitz and S. P. Cramer, Reaction Coordinate Leading to H₂ Production in [FeFe]-Hydrogenase Identified by Nuclear Resonance Vibrational Spectroscopy and Density Functional Theory, *J. Am. Chem. Soc.*, 2017, **139**, 16894–16902.
- 8 B. L. Greene, G. E. Vansuch, B. C. Chica, M. W. W. Adams and R. B. Dyer, Applications of Photogating and Time Resolved Spectroscopy to Mechanistic Studies of Hydrogenases, *Acc. Chem. Res.*, 2017, **50**, 2718–2726.
- 9 V. Fourmond, N. Plumeré and C. Léger, Reversible Catalysis, *Nat. Rev. Chem.*, 2021, **5**, 348–360.
- 10 V. Artero, G. Berggren, M. Atta, G. Caserta, S. Roy, L. Pecqueur and M. Fontecave, From Enzyme Maturation to Synthetic Chemistry: The Case of Hydrogenases, *Acc. Chem. Res.*, 2015, **48**, 2380–2387.
- 11 C. E. Foster, T. Kramer, A. F. Wait, A. Parkin, D. P. Jennings, T. Happe, J. E. McGrady and F. A. Armstrong, Inhibition of [FeFe]-Hydrogenases by Formaldehyde and Wider Mechanistic Implications for Biohydrogen Activation, *J. Am. Chem. Soc.*, 2012, **134**, 7553–7557.
- 12 A. F. Wait, C. Brandmayr, S. T. Stripp, C. Cavazza, J. C. Fontecilla-Camps, T. Happe and F. A. Armstrong, Formaldehyde—A Rapid and Reversible Inhibitor of Hydrogen Production by [FeFe]-Hydrogenases, *J. Am. Chem. Soc.*, 2011, **133**, 1282–1285.
- 13 A. Bachmeier, J. Esselborn, S. V. Hexter, T. Kramer, K. Klein, T. Happe, J. E. McGrady, W. K. Myers and F. A. Armstrong, How Formaldehyde Inhibits Hydrogen Evolution by [FeFe]-Hydrogenases: Determination by ¹³C ENDOR of Direct Fe-C Coordination and Order of Electron and Proton Transfers, *J. Am. Chem. Soc.*, 2015, **137**, 5381–5389.
- 14 H. Berke, G. Huttner, G. Weiler and L. Zsolnai, Struktur und Reaktivität eines Formaldehydeisen-Komplexes, *J. Organomet. Chem.*, 1981, **219**, 353–362.
- 15 C. P. Casey, M. W. Meszaros, S. M. Neumann, I. G. Cesa and K. J. Haller, Synthesis and X-Ray Crystal Structures of an Analog Pair of Iron Formyl and Iron Acetyl Complexes, *Organometallics*, 1985, **4**, 143–149.
- 16 K. Toyohara, K. Tsuge and K. Tanaka, Comparison of Ru-C Bond Characters Involved in Successive Reduction of Ru-CO₂ to Ru-CH₂OH, *Organometallics*, 1995, **14**, 5099–5103.
- 17 D. Schilter, J. M. Camara, M. T. Huynh, S. Hammes-Schiffer and T. B. Rauchfuss, Hydrogenase Enzymes and Their Synthetic Models: The Role of Metal Hydrides, *Chem. Rev.*, 2016, **116**, 8693–8749.
- 18 X. Zhao, I. P. Georgakaki, M. L. Miller, J. C. Yarbrough and M. Y. Darensbourg, H/D Exchange Reactions in Dinuclear Iron Thiolates as Activity Assay Models of Fe-H₂ase, *J. Am. Chem. Soc.*, 2001, **123**, 9710–9711.
- 19 J. I. van der Vlugt, T. B. Rauchfuss, C. M. Whaley and S. R. Wilson, Characterization of a Diferrous Terminal Hydride Mechanistically Relevant to the Fe-Only Hydrogenases, *J. Am. Chem. Soc.*, 2005, **127**, 16012–16013.
- 20 M. E. Carroll, B. E. Barton, T. B. Rauchfuss and P. J. Carroll, Synthetic Models for the Active Site of the [FeFe]-Hydrogenase: Catalytic Proton Reduction and the Structure of the Doubly Protonated Intermediate, *J. Am. Chem. Soc.*, 2012, **134**, 18843–18852.
- 21 P. Mathur, B. Manimaran, C. V. V. Satyanarayana and B. Varghese, Synthesis, Spectroscopic and Structural Characterisation of (CO)₆Fe₂EE'{-μ-C(H)(CH₃)₂} and (CO)₆Fe₂{μ-EC(H)(CH₃)E'} (E, E' = S, Se, Te), *J. Organomet. Chem.*, 1997, **527**, 83–91.
- 22 D. Zheng, N. Wang, M. Wang, S. Ding, C. Ma, M. Y. Darensbourg, M. B. Hall and L. Sun, Intramolecular Iron-Mediated C-H Bond Heterolysis with an Assist of Pendant Base in a [FeFe]-Hydrogenase Model, *J. Am. Chem. Soc.*, 2014, **136**, 16817–16823.
- 23 R. Zaffaroni, T. B. Rauchfuss, D. L. Gray, L. De Gioia and G. Zampella, Terminal vs. Bridging Hydrides of Diiron Dithiolates: Protonation of Fe₂(dithiolate)(CO)₂(PME₃)₄, *J. Am. Chem. Soc.*, 2012, **134**, 19260–19269.
- 24 M. T. Olsen, T. B. Rauchfuss and S. R. Wilson, Role of the Azadithiolate Cofactor in Models for [FeFe]-Hydrogenase: Novel Structures and Catalytic Implications, *J. Am. Chem. Soc.*, 2010, **132**, 17733–17740.
- 25 J. A. Wright, L. Webster, A. Jablonskyte, P. M. Woi, S. K. Ibrahim and C. J. Pickett, Protonation of [FeFe]-Hydrogenase Sub-Site Analogues: Revealing Mechanism Using FTIR Stopped-Flow Techniques, *Faraday Discuss.*, 2011, **148**, 359–371.
- 26 G. M. Chambers, S. I. Johnson, S. Raugei and R. M. Bullock, Anion Control of Tautomeric Equilibria: Fe-H vs. N-H Influenced by NH...F Hydrogen Bonding, *Chem. Sci.*, 2019, **10**, 1410–1418.
- 27 J. Emsley, Very Strong Hydrogen Bonds, *Chem. Soc. Rev.*, 1980, **9**, 91–124.
- 28 F. E. Rogers and R. J. Rapiejko, Thermochemistry of Carbonyl Addition Reactions. II. Enthalpy of Addition of Dimethylamine to Formaldehyde, *J. Phys. Chem.*, 1974, **78**, 599–603.
- 29 F. Gloaguen, J. D. Lawrence, M. Schmidt, S. R. Wilson and T. B. Rauchfuss, Synthetic and Structural Studies on [Fe₂(SR)₂(CN)_x(CO)_{6-x}]^{x-} as Active Site Models for Fe-Only Hydrogenases, *J. Am. Chem. Soc.*, 2001, **123**, 12518–12527.

- 30 P. Li, M. Wang, C. He, G. Li, X. Liu, C. Chen, B. Åkermark and L. Sun, Influence of Tertiary Phosphanes on the Coordination Configurations and Electrochemical Properties of Iron Hydrogenase Model Complexes: Crystal Structures of $[(\mu\text{-S}_2\text{C}_3\text{H}_6)\text{Fe}_2(\text{CO})_{6-n}\text{L}_n]$ ($\text{L} = \text{PMe}_2\text{Ph}$, $n = 1, 2$; PPh_3 , $\text{P}(\text{OEt})_3$, $n = 1$), *Eur. J. Inorg. Chem.*, 2005, **2005**, 2506–2513.
- 31 W.-Y. Chu, C. P. Richers, E. R. Kahle, T. B. Rauchfuss, F. Arrigoni and G. Zampella, Imine-Centered Reactions in Imino-Phosphine Complexes of Iron Carbonyls, *Organometallics*, 2016, **35**, 2782–2792.
- 32 J. A. Birrell, V. Pelmeshnikov, N. Mishra, H. Wang, Y. Yoda, K. Tamazaki, T. B. Rauchfuss, S. P. Cramer, W. Lubitz and S. DeBeer, Spectroscopic and Computational Evidence that [FeFe] Hydrogenases Operate Exclusively with CO-Bridged Intermediates, *J. Am. Chem. Soc.*, 2020, **142**, 222–232.
- 33 P. A. Butler and B. Kräutler, Biological Organometallic Chemistry of B_{12} , *Top. Organomet. Chem.*, 2006, **17**, 1–55.
- 34 J. Demarteau, A. Debuigne and C. Detrembleur, Organocobalt Complexes as Sources of Carbon-Centered Radicals for Organic and Polymer Chemistries, *Chem. Rev.*, 2019, **119**, 6906–6955.
- 35 H. Li and T. B. Rauchfuss, Iron Carbonyl Sulfides, Formaldehyde, and Amines Condense To Give the Proposed Azadithiolate Cofactor of the Fe-Only Hydrogenases, *J. Am. Chem. Soc.*, 2002, **124**, 726–727.